Journal of the Australian Ceramic Society (2022) 58:881–889
https://doi.org/10.1007/s41779-022-00736-z

RESEARCH

Sr/Ce co-immobilization evaluation and high chemical stability of novel $Sr_{0.5}Zr_2(PO_4)_3$–$CePO_4$ composite ceramics for nuclear waste forms

Junxia Wang[1] · Lei Zhan[1] · Jin Wang[1] · Jianwu Wen[1] · Linjie Fan[1] · Lang Wu[1]

Received: 3 December 2021 / Revised: 25 February 2022 / Accepted: 29 March 2022 / Published online: 10 May 2022

Abstract
Sodium zirconium phosphate (labeled as NZP)-monazite-type (1-x)$Sr_{0.5}Zr_2(PO_4)_3$–$xCePO_4$ (x = 0–1.0) composite ceramics, which were designed to simultaneously immobilize simulated fission nuclide Sr and variable valence actinide nuclide Ce, were in situ prepared by one-step microwave sintering technique. The feasibility of Sr/Ce co-immobilization was evaluated via an investigation on the phase evolution, microstructure, density, Vickers hardness, and chemical stability of the composite ceramics. The Ce valence state in the composite ceramics was further ascertained by X-ray photoelectron spectroscopy. It was shown that the Sr/Ce co-immobilized composite ceramics only consisted of $Sr_{0.5}Zr_2(PO_4)_3$ and $CePO_4$ crystalline phases that were compatible well to each other. Sr and Ce were independently incorporated into $Sr_{0.5}Zr_2(PO_4)_3$ phase and $CePO_4$ phase, respectively. The valence state of Ce in composite ceramics existed in trivalent state. And the existence of $CePO_4$ phase caused the grain refinement and facilitated the densification of the composite ceramics. The composite samples all showed a highly uniform and dense microstructure, whose relative density was higher than 95% and Vickers hardness could attain 774 HV1. Importantly, the series of $Sr_{0.5}Zr_2(PO_4)_3$–$CePO_4$ composite ceramics exhibited higher chemical stability than that of the monophase $Sr_{0.5}Zr_2(PO_4)_3$ or $CePO_4$ ceramics, in which the normalized leaching rates of Sr and Ce were below 10^{-4} g·m^{-2}·day^{-1} and 10^{-7} g·m^{-2}·day^{-1} order of magnitude, respectively. The NZP-monazite-type composite ceramics has the potential to be a host for the disposal of high-level nuclear wastes containing multiple radionuclides.

Keywords NZP-monazite-type composite ceramics · Multiple radionuclides · Immobilization · Chemical stability · Microwave sintering

Introduction

A large amount of high-level radioactive wastes (HLWs), which contain high radioactive nuclides, corrosion products, and fuel clad material, have been produced with the development of nuclear power and the decommissioning of military equipment [1]. The radionuclides in HLW include various fission products (FPs) and actinides (Ans) with multiple oxidation states, which possess long-term radiotoxicity and high corrosivity. The safe disposal and isolation of HLW to prevent the leakage and migration of radioactive nuclides is one of the key issues related to the sustainable development of nuclear power worldwide. The long-term treatment of HLW requires the selection of suitable host matrices which should have low leaching rate and high thermal, chemical, radiation, and mechanical stability under repository conditions. Ceramics, as nuclear waste solidification matrices, have been investigated for many years due to their superior properties compared with glass waste forms in terms of the chemical, thermal, and radiation resistance [2]. At present, some potential ceramics matrices, such as sodium zirconium phosphate ($NaZr_2(PO_4)_3$) [3–5], monazite [6,7], pyrochlore [8], zirconolite [9], and apatite [10], have been extensively concerned during recent years. However, most ceramics matrices are only suitable for accommodating a certain FP or An radionuclide due to the finiteness of their lattice substitution, which limits the application of these ceramics

✉ Junxia Wang
wjunxia2002@163.com

✉ Jin Wang
wjin761026@163.com

[1] School of Materials Science and Engineering, Southwest University of Science and Technology, Mianyang 621010, China

matrices in immobilizing HLW containing various FP and An radionuclides. As to this problem, it may be a feasible approach to utilize the multiphase composite ceramics to concurrently immobilize FP and An with diverse valences and ionic radius.

In the last few decades, the research on the multiphase composite ceramics for the HLW immobilization mostly focuses on titanate-based ceramic waste forms. Among these composite ceramics, the multiphase titanate-based ceramics targeting hollandite, zirconolite/pyrochlore, and perovskite phases have been extensively investigated on the preparation [11], irradiation stability [12], and chemical durability [13,14]. It was reported that Cr addition can facilitate the formation and stability of a Cs-containing hollandite phase in the kind of multiphase ceramics prepared by melt process [11]. Clark et al. revealed the chemical durability of multiphase ceramic designer waste forms could be improved by adjusting the phase proportion. It was found that the fractional Cs release decreased as the amount of hollandite phase increased; however, the zirconolite and pyrochlore phases did not significantly contribute to the elemental release from the hollandite phase [14]. In addition, hollandite–perovskite composite ceramics could be also considered a customized host matrix for immobilization of the separated Cs and Sr from HLW streams, exhibiting excellent chemical durability [15]. Besides, zirconolite–sphene composite ceramics were explored for immobilizing tetravalent actinide U, which was incorporated in the Zr site of zirconolite and in the Ca site of sphene [16]. Similarly, tetravalent actinide Ce could be simultaneously immobilized in Zr site of zirconia phase and zircon phase in $0.2Zr_{1-x}Ce_xO_2/Zr_{1-y}Ce_ySiO_4$ ceramics [17]. The SiC–$MgAl_2O_4$ composite ceramic was intended to immobilize ^{14}C and other high-level radioactive nuclides, which was reported by Teng YC [18,19]. It was found that $MgAl_2O_4$ phase, as a matrix for immobilizing long-lived nuclides, could improve the sintering of SiC ceramics, and the SiC–$MgAl_2O_4$ composite ceramics presented good physical and chemical stability. Thus, the multiphase composite ceramics can provide the flexibility, selectivity, and high loading for radionuclides by combining with the structural advantages of their respective crystalline phases. Considering the better practical application and performance of composite ceramics than those of single-phase ceramics, it is essential to develop new composite ceramics to immobilize complex high-level radionuclides with diverse valences and ionic radius [20].

NZP family compounds, whose crystalline structure is composed of three-dimensional hexagonal framework of PO_4 tetrahedra sharing corners with ZrO_6 octahedra [21], are well known for its ionic conductivity, low thermal expansion, and flexibility on ionic substitution [22,23]. As a potential host, the NZP-type ceramics are widely studied for immobilizing FP radionuclides (^{90}Sr/ ^{137}Cs) due to its abundant ionic substitution. For instance, Hashimoto et al. investigated the immobilization process of Cs and Sr into $HZr_2(PO_4)_3$ by using an autoclave [24]. Pet'kov et al. reported the thermophysical properties and hydrolytic stability of $Sr_{0.5}Zr_2(PO_4)_3$ for immobilizing ^{90}Sr [25]. Meanwhile, as the host for FP radionuclide (^{90}Sr/^{137}Cs) immobilization, NZP family presented high chemical stability, as well as radiation resistance properties [3,26]. Monazite, an anhydrous monoclinic rare-earth orthophosphate mineral ($REPO_4$) consisting of distorted PO_4 tetrahedra and REO_9 polyhedra, is a high-profile matrix for the disposal of trivalent and tetravalent An radionuclides due to the flexibility of REO_9 polyhedral structure. This kind ceramic waste forms present the excellent mechanical, thermal and chemical properties, and high radionuclide loading capacity as well as superior radiation resistance [27]. Besides, it was also previously reported that the monazite-zirconium phosphate–type composite ceramics worked well as a matrix to immobilize HLW, especially to decrease the leaching rate of alkali and alkaline ions [28]. Similarly, the presence of monazite did not deteriorate the aqueous stabilities of NZP ceramics [29]. So NZP-monazite-type composite ceramics would be an applicable matrix for immobilizing complex HLW containing FP and An with multiple valence, on which there are few reports so far [20,30]. In particular, the proportion of NZP and monazite phases in NZP-monazite-type composite ceramics can be adjusted for the requirement of simultaneously immobilizing FP and An radionuclides of indefinite quantity. Thus, by comparison with other ceramic waste forms previously reported, the novel NZP-monazite-type composite ceramics proposed in this work may have potential application advantages in immobilizing HLW.

In this work, Sr and Ce from the raw materials of $Sr(NO_3)_2$ and CeO_2 were introduced as the surrogates for the fission nuclide ^{90}Sr and variable valence actinide nuclide (trivalent valence and tetravalent valence actinide), respectively. The chemical formula of NZP-monazite-type composite ceramics was designed as $(1-x)Sr_{0.5}Zr_2(PO_4)_3-xCePO_4$ ($x=0$, 0.2, 0.4, 0.6, 0.8, and 1.0). The series of $Sr_{0.5}Zr_2(PO_4)_3$–$CePO_4$ composite samples were in situ prepared by one-step microwave sintering technique in this work. The synthesis of crystalline phases and the sintering of composite ceramics were concurrently achieved in microwave processing of the in situ preparation, which was different from the conventional preparation process of composite ceramics [31,32]. The evolution of phase composition, microstructure, physical properties, and chemical stability of the as-prepared samples were systematically investigated. It was aimed to discuss the feasibility of $(1-x)Sr_{0.5}Zr_2(PO_4)_3$–$xCePO_4$ composite ceramic waste forms for simultaneously immobilizing FP and An. In addition, the valence state of variable valence Ce in the as-prepared composite ceramics was also analyzed.

Experimental

Preparation of samples

$(1-x)Sr_{0.5}Zr_2(PO_4)_3$–$xCePO_4$ composite ceramics ($x=0$, 0.2, 0.4, 0.6, 0.8, and 1.0) were prepared by using $Sr(NO_3)_2$ (99.0%) in appropriate amounts and CeO_2 (99.99%), ZrO_2 (99.0%), and $NH_4H_2PO_4$ (99.0%) in high purity as the starting materials and by employing one-step microwave sintering technique. To be specific, the starting materials were weighted by stoichiometric ratios and then thoroughly ball-mill mixed and ground. The mixture powders were preheated at 600 °C holding for 8 h in a muffle furnace to decompose $Sr(NO_3)_2$ and $NH_4H_2PO_4$ for emission of nitrogen dioxide, ammonia, and water vapors [33]. Subsequently, the preheated powders were again ball-milled together with adding the sintering aid of 1.0 wt% ZnO powders. After being dried and passed through a 200-mesh sieve, the resultant powders were pressed into Ø12 × 2 mm tablets by cold isostatic pressing under 200 MPa. Finally, the green compacts were microwave sintered at different temperatures (1050 ~ 1200 °C) for 2 h with a heating rate of 5 °C/min by a multi-mode of 2.45-GHz, 4-kW commercial microwave workstation (MobileLab Workstation, Tangshan Nayuan Microwave Thermal Instrument Manufacturing Co. Ltd., China). Thus, the series of composite ceramics waste forms for immobilizing radionuclides Sr and Ce were obtained.

Characterization

Thermogravimetry–differential scanning calorimetry (TG-DSC, SDT Q600, TA, USA) analysis of the preheated powders was performed under nitrogen atmosphere with a heating rate of 10 °C/min. The phase evolution with varying components was examined by powder X-ray diffraction (XRD, DMAX1400, Rigaku Inc., Japan) using Cu-Kα radiation. The microstructures and chemical compositions of the samples were acquired by scanning electron microscopy (SEM) attached with an energy-dispersive spectrometer (EDS) (SEM–EDS, Hitachi TM-4000, Japan). The binding energy and oxidation state of the composite ceramics ($x=0.2$–0.8) were analyzed by X-ray photoelectron spectroscopy (XPS, ESCALAB 250Xi, Thermo Scientific, USA) using Al-Kα radiation with a step size of 0.05 eV. The ion-electronic charge compensation system was used to neutralize the charge of the sample in the experiments. All peaks were calibrated against the C1s peak at 284.8 eV. The XPS spectra were analyzed using the software XPSPEAK41. The bulk density (ρ) of the as-prepared samples was obtained via the Archimedes method. The relative density was calculated using the formula of $\rho/\rho_0 \times 100\%$, in which ρ_0 denotes theoretical density. The specific calculation process was carefully introduced in our previous work [34]. The Vickers hardness (HV) of the samples was measured by the indentation fracture technique utilizing a Vickers 136°-diamond indenter (HVS-1000Z, Shanghai Wanheng Precision-instrument Co., Ltd., China) with 1 kgf load for 10 s. The HV results were averaged from three samples and each sample was tested five times, whose value was dimensionsless unit and HV1 refers to the HV test with 1kgf load.

Chemical stability

The chemical stability of typical $(1-x)Sr_{0.5}Zr_2(PO_4)_3-xCePO_4$ ($x=0$, 0.4, 0.6, and 1.0) samples was investigated by the Product Consistency Test (PCT) which is a standard static leaching method from ASTM C1285-14 [35]. The sintered samples were smashed and screened out the powders between 100 and 200 mesh, and then washed by absolute ethanol and ultrapure water. A certain proportion of the as-obtained powders and deionized water was put into a well-sealed hydrothermal reaction kettle (304 stainless steel shell and teflon container), and held at 90 °C for 7 days. The concentration of Sr, Ce, Zr, and P in the leaching solution was measured by inductively coupled plasma optical emission spectroscopy (ICP-OES, Thermo iCAP6500, Thermo Fisher, USA). The normalized elemental leach rates (LR_i) were calculated according to the following formula [36,37]:

$$LR_i = \frac{C_i \bullet V}{f_i \bullet A_s \bullet \Delta t} \quad (1)$$

where C_i is the concentration of element i in the leaching solution (g/m^3), V is the volume of the leaching solution (m^3), f_i is the mass fraction of element i in the sample (wt%), A_s is the geometric surface area of the sample (m^2), and Δt is the leaching time (day).

Results and discussion

TG-DSC analysis

To determine the suitable sintering temperature of the composite ceramics, the TG-DSC analysis of the typical preheated powders corresponding to $0.6Sr_{0.5}Zr_2(PO_4)_3$–$0.4CePO_4$ component is performed, whose curves are shown in Fig. 1. As seen in Fig. 1, the total weight loss of the preheated powders is about 1.8% and 5.1% in the ranges of room temperature to 350 °C and 350 to 400 °C, respectively, which is associated with the dehydration of free water and

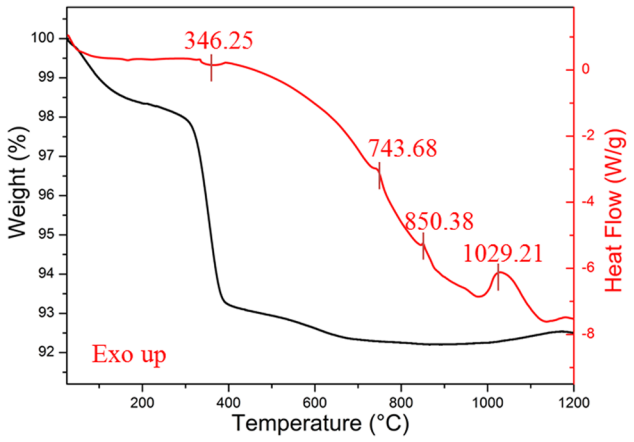

Fig. 1 TG-DSC curves of the preheated powders of $0.6Sr_{0.5}Zr_2(PO_4)_3$–$0.4CePO_4$ composition

bound water of the powders. Meanwhile, the endothermic peak at 346.25 °C on the DSC curve is caused by the dehydration of bound water. The weight loss of approximately 0.8% at the temperature range of 400–650 °C may be attributed to incomplete decomposition of raw material powders after preheating treatment. Clearly, three exothermic peaks at 743.7, 850.4, and 1029.2 °C are observed on the DSC curve, but no obvious weight loss at the corresponding temperatures is found from TG curve. It is inferred that $CePO_4$ phase and $Sr_{0.5}Zr_2(PO_4)_3$ phase are synthesized at 743.7 °C and 850.4 °C, respectively. The sintering densification of the composite ceramics may be proceeded at 1029.2 °C, which also corresponds to the work temperature of ZnO sintering aid [[[24]]]. Thus, the sintering temperature ranging from 1050 to 1200 °C was preliminarily chosen on the basis of the TG-DSC analysis.

Evolution of the phase composition

The powder XRD patterns of $0.6Sr_{0.5}Zr_2(PO_4)_3$–$0.4CePO_4$ sample after microwave sintering at 1050–1200 °C for 2 h are shown in Fig. 2a. From Fig. 2a, it can be seen that the $0.6Sr_{0.5}Zr_2(PO_4)_3$–$0.4CePO_4$ sample sintered at different temperatures all shows the characteristic diffraction peaks of crystalline $Sr_{0.5}Zr_2(PO_4)_3$ phase (JCPDS PDF#33–1360) and $CePO_4$ phase (JCPDS PDF#32–0199). The crystallization peak strength and peak width slightly change as the sintering temperature varies from 1050 to 1200 °C. It is indicated that the two crystalline phases are relatively stable and the composite ceramics can be in situ prepared in a wide temperature range. Considering the energy consumption during sintering process, the $(1-x)Sr_{0.5}Zr_2(PO_4)_3$–$xCePO_4$ samples ($x=0$–1.0) for subsequent analyses were prepared at the lowest sintering temperature (1050 °C) in this work. The powder XRD patterns of the samples sintered at 1050 °C for 2 h are presented in Fig. 2b. As seen in Fig. 2b, the $(1-x)Sr_{0.5}Zr_2(PO_4)_3$–$xCePO_4$ samples show the characteristic diffraction peaks of pure $Sr_{0.5}Zr_2(PO_4)_3$ phase and pure $CePO_4$ phase for x value are 0 and 1.0, respectively. Besides, the phase composition of the composite ceramic samples ($x=0.2$–0.8) only contains $Sr_{0.5}Zr_2(PO_4)_3$ phase and $CePO_4$ phase and no other crystalline phases are found. As expected, the diffraction peak intensity of $Sr_{0.5}Zr_2(PO_4)_3$ phase just decreases regularly as the x value raises, whereas that of $CePO_4$ phase gradually increases. Based on the XRD results, it is confirmed that there is no noticeable chemical reactions between $Sr_{0.5}Zr_2(PO_4)_3$ and $CePO_4$ phases, which reflects the stability and compatibility of the two crystalline phases.

Analysis of valence state of Ce

Ce is a good surrogate for actinides radionuclide Pu with multiple oxidation states. In order to ascertain the valence states of Ce element in the prepared composite ceramics, XPS test was performed on $(1-x)Sr_{0.5}Zr_2(PO_4)_3$–$xCePO_4$ composite ceramic samples ($x=0.2$–0.8), whose high resolution Ce 3d XPS spectra are shown in Fig. 3. It is well known that the electrons of Ce atom have spin–orbit interaction, causing the energy split. Thus, the XPS spectra consist of two pairs of spin–orbit split peaks and associated shake-up satellites (denoted as u_0/u_0' and u_1/u_1', respectively). The components u_0 and u_1 refer to

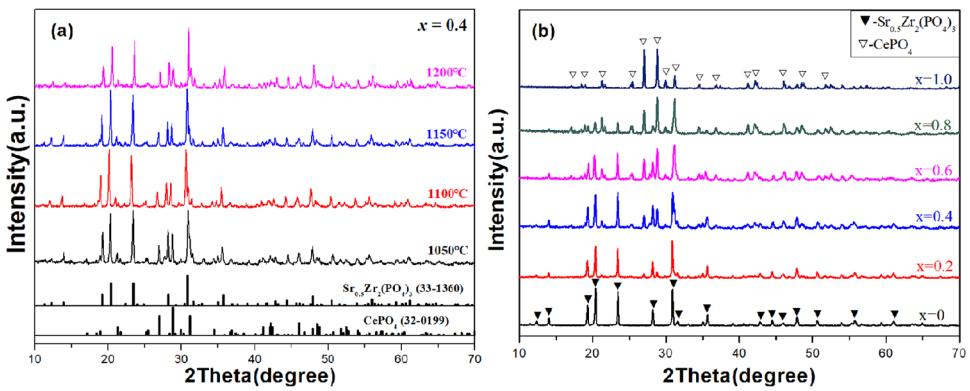

Fig. 2 XRD patterns of $(1-x)Sr_{0.5}Zr_2(PO_4)_3$–$xCePO_4$ composite ceramics: **a** $x=0.4$ sample after microwave sintering at different temperatures for 2 h; **b** $x=0$–1.0 samples after microwave sintering at 1050 °C for 2 h

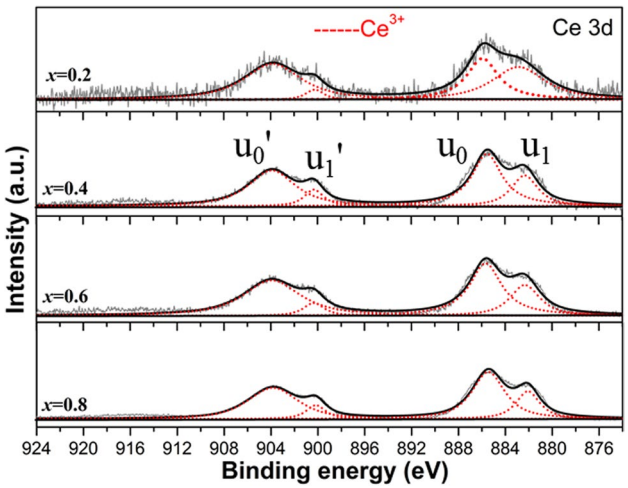

Fig. 3 High-resolution Ce 3d XPS spectra of $(1-x)Sr_{0.5}Zr_2(PO_4)_3$–$xCePO_4$ composite ceramics

$3d_{5/2}$, while u_0' and u_1' stand for $3d_{3/2}$, which all indicates the presence of Ce^{3+}. As shown in Fig. 3, the peaks at 882.0, 885.5, 900.1, and 903.8 eV are clearly seen, corresponding to u_1, u_0, u_1', and u_0', respectively. However, the peak around 916.3 eV, which is considered a marker for the presence of Ce^{4+} [38], is almost unobserved. Then, it is verified that the valence state of Ce in the as-prepared composite ceramics mainly exists in trivalent state, which is in accord with the valence state of Ce in $CePO_4$ phase.

Micromorphology analysis

Figure 4 shows the backscattered electron SEM images of the fracture surfaces of $(1-x)Sr_{0.5}Zr_2(PO_4)_3$–$xCePO_4$ samples. It is clearly found that all samples present a well-densified microstructure. By comparison, the pure $Sr_{0.5}Zr_2(PO_4)_3$ sample ($x=0$) presents transgranular fracture (Fig. 4a), while the pure $CePO_4$ sample ($x=1$) shows the characteristic of intercrystalline fracture (Fig. 4f). It implies that the sintering densification of $Sr_{0.5}Zr_2(PO_4)_3$ sample is superior than that of $CePO_4$ sample. Nonetheless, the $CePO_4$ sample still possesses a dense microstructure with closely packed crystal grains. As shown in Fig. 4b–e, the composite ceramics ($x=0.2$–0.8) also exhibit the characteristic of transgranular fracture and the crystalline grains of the samples show different brightness and sizes, which can be clearly differentiated by the contrast of their morphologies. According to the above XRD results and the imaging features of SEM, the bigger and darker grains might be related to $Sr_{0.5}Zr_2(PO_4)_3$ phase, and the smaller and brighter grains might be correlated with $CePO_4$ phase. Obviously, the two phases are evenly distributed in the composite ceramics. Additionally, the crystalline sizes of the composite ceramic samples are all obviously smaller than that of pure $Sr_{0.5}Zr_2(PO_4)_3$ sample and $CePO_4$ sample, though the $CePO_4$ grain size gradually grows with the increasing x value. That is to say, the existence of $CePO_4$ phase brought about the grain refinement and could facilitate the densification of the composite ceramics.

Figure 5 displays the SEM–EDS elemental distribution mapping of the representative $0.6Sr_{0.5}Zr_2(PO_4)_3$–$0.4CePO_4$

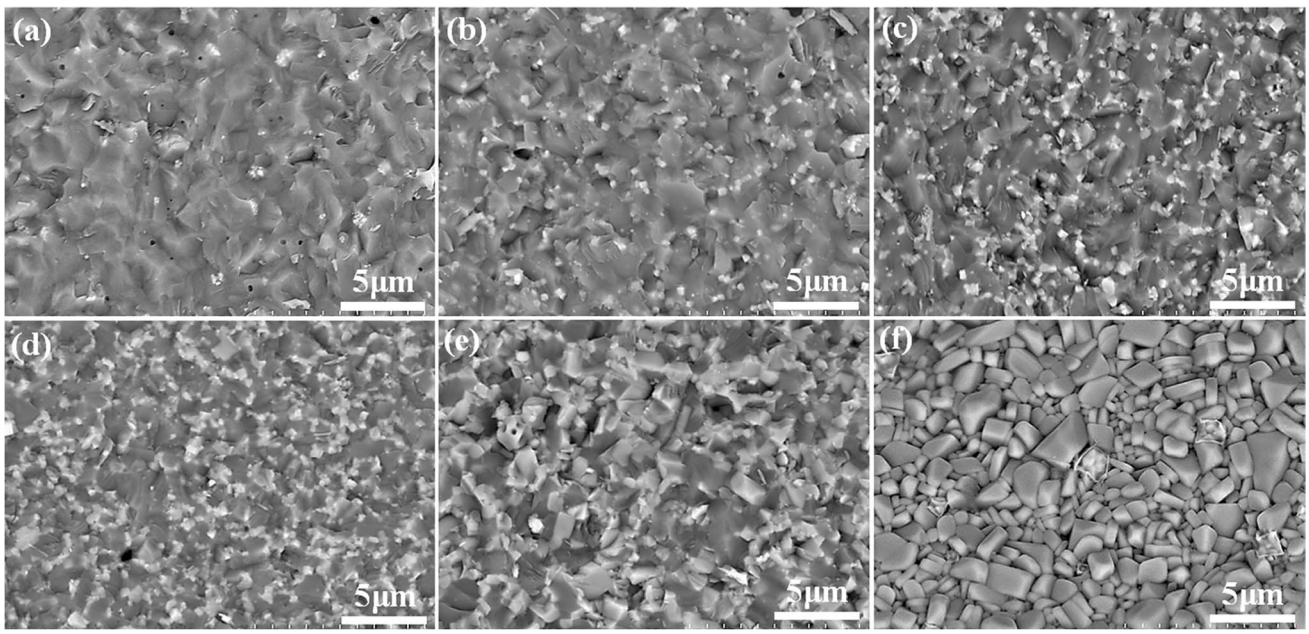

Fig. 4 SEM images of $(1-x)Sr_{0.5}Zr_2(PO_4)_3$–$xCePO_4$ composite ceramics: **a** $x=0$; **b** $x=0.2$; **c** $x=0.4$; **d** $x=0.6$; **e** $x=0.8$; **f** $x=1.0$

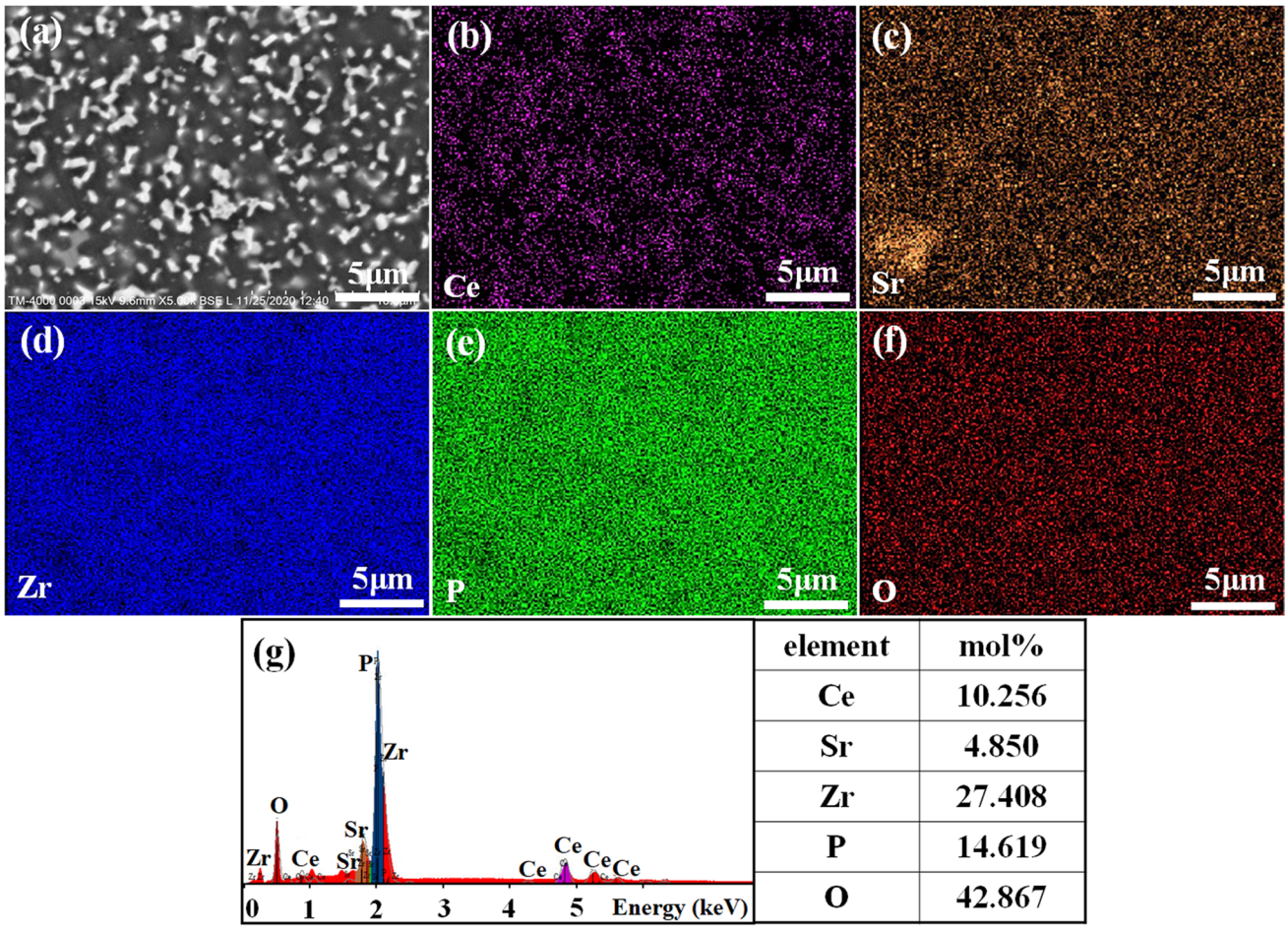

element	mol%
Ce	10.256
Sr	4.850
Zr	27.408
P	14.619
O	42.867

Fig. 5 SEM–EDS elemental mapping of $0.6Sr_{0.5}Zr_2(PO_4)_3$–$0.4CePO_4$ composite ceramics

sample. To be specific, Fig. 5a represents the polished surface SEM image of the sample and Fig. 5b–f show the results of EDS elemental mapping, in which the chemical compositions of the sample are composed of Ce, Sr, Zr, P, and O. It is clear that Ce elemental distribution mapping (Fig. 5b) is just correlated with the brighter $CePO_4$ phase in Fig. 5a, while Sr elemental distribution mapping (Fig. 5c) is associated with the darker $Sr_{0.5}Zr_2(PO_4)_3$ phase. Besides, on the basis of the elemental atomic ratios listed in the table (embedded in Fig. 5g), the calculated atomic ratios of P/O and Sr/Ce/Zr are 14.62/42.87 and 4.85/10.26/27.41, respectively, which are very close to the theoretical stoichiometric atomic ratios of [PO_4] (1:4) and $0.6Sr_{0.5}Zr_2(PO_4)_3$–$0.4CePO_4$ formula (Sr/Ce/Zr is about 3:4:12). The SEM–EDS results further proved that Sr and Ce radionuclides were independently incorporated into the crystalline lattices of $Sr_{0.5}Zr_2(PO_4)_3$ and $CePO_4$ phases in the composite ceramics waste forms.

Density and Vickers hardness analyses

To further investigate the physical properties of the as-prepared composite ceramics, the density and Vickers hardness of $(1-x)Sr_{0.5}Zr_2(PO_4)_3$–$xCePO_4$ samples are tested and their results are given in Fig. 6a and b, respectively. It is found in Fig. 6a that the bulk density of $(1-x)Sr_{0.5}Zr_2(PO_4)_3$–$xCePO_4$ sample ($x=0$–1.0) increases gradually as x value rises, from 3.27 g/cm^3 of pure $Sr_{0.5}Zr_2(PO_4)_3$ sample ($x=0$) to 4.96 g/cm^3 of pure $CePO_4$ sample ($x=1.0$), which well conforms to the compound effect regulation. For $Sr_{0.5}Zr_2(PO_4)_3$–$CePO_4$ composite samples, the calculated relative densities are all greater than 95%, even up to 97.7%. By comparison, the relative densities of all composite samples are almost higher than that of pure $CePO_4$ sample and also comparable with that of pure $Sr_{0.5}Zr_2(PO_4)_3$ sample. The densification analyses are in good agreement with SEM results. Just as expected from the above SEM results, the dense NZP-monazite-type composite ceramics waste forms can be achieved by on-site

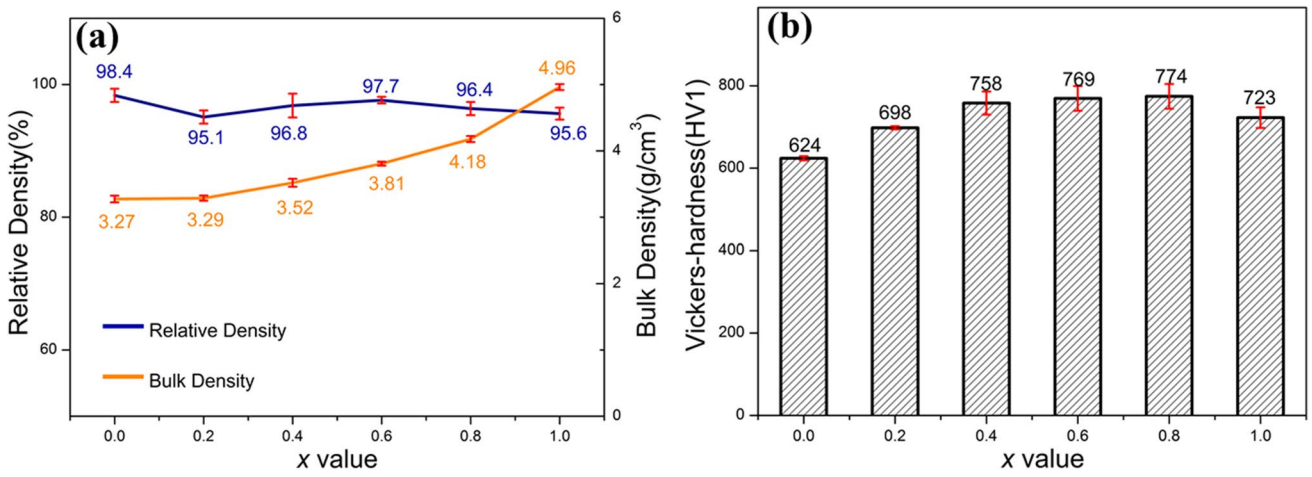

Fig. 6 Density and Vickers-hardness of $(1-x)Sr_{0.5}Zr_2(PO_4)_3$–$xCePO_4$ composite ceramics

preparation in this work. Figure 6b shows that the Vickers hardness of pure $Sr_{0.5}Zr_2(PO_4)_3$ sample ($x=0$) is 624 HV1, and the Vickers hardness of the $(1-x)Sr_{0.5}Zr_2(PO_4)_3$–$xCePO_4$ composite sample gradually increases as the x value goes up from 0.2 to 0.8. When the x value is 0.8, the $0.2Sr_{0.5}Zr_2(PO_4)_3$–$0.8CePO_4$ sample accomplishes the highest hardness of 774 HV1. However, pure $CePO_4$ sample ($x=1.0$) only presents the Vickers hardness of 723 HV1. Notably, the introduction of $CePO_4$ phase not only promotes the densification of the $Sr_{0.5}Zr_2(PO_4)_3$–$CePO_4$ composite ceramics but also improves their Vickers hardness. According to the above analyses, it is inferred that the introduction of $CePO_4$ phase could refine $Sr_{0.5}Zr_2(PO_4)_3$ grains and then strengthen grain interfaces of the composite ceramics without decreasing their densification. Thus, as the $CePO_4$ phase increases, the grain refinement effect and the good densification would jointly improve the hardness of $Sr_{0.5}Zr_2(PO_4)_3$–$CePO_4$ composite ceramics, which is beneficial for the shock resistance of $Sr_{0.5}Zr_2(PO_4)_3$–$CePO_4$ composites as nuclear waste form.

Chemical stability of composite ceramics

The typical $(1–x)Sr_{0.5}Zr_2(PO_4)_3$–$xCePO_4$ ($x=0$, 0.4, 0.6, and 1.0) samples were conducted by PCT leaching test at 90 °C for 7 days to evaluate their chemical stability. The normalized leaching rates LR_i ($i=$ Sr, Ce, Zr, and P) of the samples are presented in Table 1. It is evident that the normalized elemental leaching rates of all samples are quite low, which may be related to the stable crystalline structures of NZP family and monazite as well as the high densification of the samples. By contrast, the values of LR_{Ce} and LR_{Zr} are significantly lower than those of LR_{Sr} and LR_P, which is mainly due to the more stable and stronger Ce–O bond of $[CeO_9]$ polyhedron in $CePO_4$ crystalline structure and Zr–O bond of $[ZrO_6]$ octahedron in $Sr_{0.5}Zr_2(PO_4)_3$ crystalline structure. In addition, the LR_{Sr} ($<4.142\times10^{-4}$ g·m^{-2}·day^{-1}), LR_{Zr} ($<2.191\times10^{-7}$ g·m^{-2}·day^{-1}), and LR_P ($<1.014\times10^{-4}$ g·m^{-2}·day^{-1}) of the composite ceramics ($x=0.4$, 0.6) are all lower 1–2 orders of magnitude than that of the monophase ceramics, especially for $Sr_{0.5}Zr_2(PO_4)_3$ ceramics. The above LR_i results of composite ceramics indicated that the introduction of $CePO_4$ phase could improve the chemical stability of $Sr_{0.5}Zr_2(PO_4)_3$ phase in the composite ceramics. It may be attribute to the uniform and grain-refined microstructure as well as the excellent densification of the $Sr_{0.5}Zr_2(PO_4)_3$–$CePO_4$ composite ceramics with the introduction of $CePO_4$ phase. Thus, compared with the monophase ceramics, the composite ceramics present a better chemical stability, although the LR_{Ce} ($<4.676\times10^{-7}$ g·m^{-2}·day^{-1}) of the composite samples is slightly higher than the LR_{Ce} ($<7.038\times10^{-8}$ g·m^{-2}·day^{-1}) of pure $CePO_4$ sample. According to the PCT leaching test

Table 1 Normalized elemental leaching rates of $(1-x)Sr_{0.5}Zr_2(PO_4)_3$–$xCePO_4$ ($x=0$, 0.4, 0.6, and 1.0) composite ceramics

Sample		LR_i/g·m^{-2}·day^{-1}			
		Sr	Zr	P	Ce
$x=0$	$Sr_{0.5}Zr_2(PO_4)_3$	5.716E-03	2.548E-06	1.193E-03	/
$x=0.4$	$0.6Sr_{0.5}Zr_2(PO_4)_3$–$0.4CePO_4$	3.375E-04	1.005E-08	9.152E-05	3.244E-07
$x=0.6$	$0.4Sr_{0.5}Zr_2(PO_4)_3$–$0.6CePO_4$	4.142E-04	2.191E-07	1.014E-04	4.676E-07
$x=1$	$CePO_4$	/	/	3.693E-04	7.038E-08

results, it is suggested that the in situ prepared $(1-x)Sr_{0.5}Zr_2(PO_4)_3$–$xCePO_4$ composite ceramics waste forms possess the superior chemical stability and the NZP-monazite-type composite ceramics could be qualified as a potential host for immobilizing HLW.

Conclusions

The $(1-x)Sr_{0.5}Zr_2(PO_4)_3$–$xCePO_4$ ($x=0$–1.0) composite ceramics for simultaneously immobilizing Sr and Ce radionuclides were in situ prepared via one-step microwave sintering technique. The composite ceramics were composed of $Sr_{0.5}Zr_2(PO_4)_3$ and $CePO_4$ phases that were stable and compatible well. As the surrogates for fission product and variable trivalent/tetravalent actinides, the simulated radionuclides of Sr and Ce were independently immobilized into $Sr_{0.5}Zr_2(PO_4)_3$ phase and $CePO_4$ phase, respectively. The valence state of Ce in the as-prepared composite ceramics existed in trivalent state. The $Sr_{0.5}Zr_2(PO_4)_3$ phase and $CePO_4$ phase were evenly distributed in the composite ceramics and the existence of $CePO_4$ phase brought about the grain refinement. Moreover, the $Sr_{0.5}Zr_2(PO_4)_3$–$CePO_4$ composite ceramics possessed the excellent densification with the relative density all above 95% and the high Vickers hardness up to 774 HV1. The PCT leaching test results showed that the $Sr_{0.5}Zr_2(PO_4)_3$–$CePO_4$ composite ceramics exhibited the better chemical stability than the $Sr_{0.5}Zr_2(PO_4)_3$ or $CePO_4$ monophase ceramics. It is suggested that NZP-monazite-type composite ceramics could be a potential host for the co-immobilization of fission products and actinide nuclides with diverse valences and ionic radius.

Funding This work was financially supported by the National Natural Science Foundation of China (Nos. 11705153 and 12075195).

Declarations

Conflict of interest The authors declare no competing interests.

References

1. Ewing, R.C.: Radiation effects in nuclear waste forms for high-level radioactive waste. Prog. Nucl. Energ. **29**, 63–127 (1995)
2. Donald, I.W.: Waste immobilization in glass and ceramic based hosts: radioactive, toxic and hazardous wastes. Tetrahedron Lett. **38**, 4199–4202 (2010)
3. Wei, Y.F., Luo, P., Wang, J.X., Wen, J.W., Zhan, L., Zhang, X., Yang, S.Y., Wang, J.: Microwave-sintering preparation, phase evolution and chemical stability of $Na_{1-2x}Sr_xZr_2(PO_4)_3$ ceramics for immobilizing simulated radionuclides. J. Nucl. Mater. **540**, 152366 (2020)
4. Bohre, A., Shrivastava, O.: Crystallographic evaluation of sodium zirconium phosphate as a host structure for immobilization of cesium and strontium. Int. J. Appl. Ceram. Tec. **10**, 552–563 (2013)
5. Bykov, D.M., Gobechiya, E.R., Kabalov, Y.K., Orlova, A.I., Tomilin, S.V.: Crystal structures of lanthanide and zirconium phosphates with general general formula $Ln_{0.33}Zr_2(PO_4)_3$, where Ln=Ce, Eu, Yb. J. Solid. State Chem. **179**, 3101–3106 (2006)
6. Potanina, E., Golovkina, L., Orlova, A., Nokhrin, A., Boldin, M., Sakharov, N.: Lanthanide (Nd, Gd) compounds with garnet and monazite structures. Powders synthesis by "wet" chemistry to sintering ceramics by Spark Plasma Sintering. J. Nucl. Mater. **473**, 93–98 (2016)
7. Rawat, D., Phapale, S., Mishra, R., Dash, S.: Thermodynamic investigation of thorium and strontium substituted monazite solid-solution. Thermochim. Acta **674**, 10–20 (2019)
8. Zhang, Y.T., Huang, Z.Y., Qi, J.Q., Han, Y., Tang, Z., Wei, H., Duan, J.J., Zeng, Y.Y., Zhang, H.B., Lu, T.C.: Rapid fabrication of fine-grained $Gd_{2-x}Nd_xZr_{2-5x}Ce_{5x}O_7$ ceramics by microwave sintering. J. Alloys. Compounds **781**, 710–715 (2019)
9. Helean, K.B., Navrotsky, A., Lian, J., Ewing, R.C.: Thermochemical investigations of zirconolite, pyrochlore and brannerite: candidate materials for the immobilization of plutonium. MRS Proc. **807**, 297 (2003)
10. Chartier, A., Meis, C., Gale, J.D.: Computational study of Cs immobilization in the apatites $Ca_{10}(PO_4)_6F_2$, $Ca_4La_6(SiO_4)_6F_2$ and $Ca_2La_8(SiO_4)_6O_2$. Phys. Rev. B **64**, 085110 (2001)
11. Amoroso, J., Marra, J.C., Tang, M., Lin, Y., Chen, F., Su, D., Brinkman, K.S.: Melt processed multiphase ceramic waste forms for nuclear waste immobilization. J. Nucl. Mater. **454**, 12–21 (2014)
12. Clark, B.M., Tumurgoti, P., Sundaram, S.K., Amoroso, J.W., Marra, J.C., Shutthanandan, V., Tang, M.: Radiation damage of hollandite in multiphase ceramic waste forms. J. Nucl. Mater. **494**, 61–66 (2017)
13. Harkins, D.H.: The durability of single, dual, and multiphase titanate ceramic waste forms for nuclear waste immobilization, Masters Thesis, Clemson University, Clemson, SC (2016)
14. Clark, B.M., Tumurgoti, P., Sundaram, S.K., Amoroso, J.W., Marra, J.C.: Preparation and characterization of multiphase ceramic designer waste forms. Sci. Rep. **11**, 4512 (2021)
15. Ma, J., Fang, Z.W., Yang, X.Y., Wang, B., Luo, F., Zhao, X.L., Wang, X.F., Yang, Y.S.: Investigating hollandite-perovskite composite ceramics as a potential waste form for immobilization of radioactive cesium and strontium. J. Mater. Sci. **56**, 9644–9654 (2021)
16. Teng, Y.C., Wang, S.L., Wu, L., Gui, C.M.: Synthesis and hydrothermal stability of U doped zirconolite–sphene composite materials. Adv. Appl. Ceram. **114**, 9–13 (2015)
17. Ding, Y., Jiang, Z.D., Xiong, T.H., Bai, Z.M., Zhao, D.D., Dan, H., Duan, T.: Phase and microstructure evolution of $0.2Zr_{1-x}Ce_xO_2/Zr_{1-y}Ce_ySiO_4$ ($0\leq x+y\leq 1$) ceramics designed to immobilize tetravalent actinides. J. Nucl. Mater. **539**, 152318 (2020)
18. Teng, Y.C., Wang, Q., Wu, L., Zhao, X.F., Chen, Y., Cao, X., Wang, W.: Effect of reactivity of silicon and magnesium on the preparation of SiC-$MgAl_2O_4$ composites for immobilizing graphite. Ceram. Int. **45**, 10203–10210 (2019)
19. Wang, Q., Teng, Y.C., Wu, L., Zhang, K.B., Zhao, X.F., Hu, Z.: Synthesis and characterization of SiC based composite materials for immobilizing radioactive graphite. J. Nucl. Mater. **504**, 94–100 (2018)
20. Wang, L., Liang, T.X.: Ceramics for high level radioactive waste solidification. J. Adv. Ceram. **1**, 194–203 (2012)
21. Hagman, L., Kierkegaard, P., Karvonen, P., Virtanen, A.I., Paasivirta, J.: The crystal structure of $NaMe_2^{IV}(PO_4)_3$; Me^{IV}= Ge, Ti. Zr. Acta Chem. Scand. **22**, 1822–1832 (1968)

22. Mutter, D., Urban, D.F., Elsässer, C.: Computational analysis of composition- structure- property- relationships in NZP-type materials for Li-ion batteries. J. Appl. Phys. **125**, 215115 (2019)
23. Wang, Y., Zhou, Y.Y., Han, Z.Q., Liu, F.T.: Investigation and characterization of crystal structure, mechanical and thermophysical properties of $CaZr_{4-x}Ti_xP_6O_{24}$ ceramics. Ceram. Int. **45**, 10596–10602 (2019)
24. Hashimoto, C., Nakayama, S.: Immobilization of Cs and Sr to $HZr_2(PO_4)_3$ using an autoclave. J. Nucl. Mater. **396**, 197–201 (2010)
25. Pet'kov, V., Asabina, E., Loshkarev, V., Sukhanov, M.: Systematic investigation of the strontium zirconium phosphate ceramic form for nuclear waste immobilization. J. Nucl. Mater. **471**, 122–128 (2016)
26. Gregg, D.J., Karatchevtseva, I., Thorogood, G.J., Davis, J., Bell, B.D.C., Jackson, M., Dayal, P., Ionescu, M., Triani, G., Short, K., Lumpkin, G.R., Vance, E.R.: Ion beam irradiation effects in strontium zirconium phosphate with NZP-structure type. J. Nucl. Mater. **446**, 224–231 (2014)
27. Schlenz, H., Heuser, J., Neumann, A., Schmitz, S., Bosbach, D.: Monazite as a suitable actinide waste form,Z. Krist.-Cryst. Mater. **228**, 113–123 (2013)
28. Ishida, M., Yanagi, Y., Terai, T.R.: Leach rates of composite waste forms of monazite- and zirconium phosphate-type. J. Nucl. Sci. Technol. **24**, 404–408 (1987)
29. Orlova, A., Kitaev, D.: Phosphate monazite- and $NaZr_2(PO_4)_3$ (NZP)-like ceramics containing uranium and plutonium. Czech. J. Phys. **53**, 665–670 (2003)
30. Orlova, A.L., Ojovan, M.I.: Ceramic mineral waste-Forms for nuclear waste immobilization. Materials **12**, 2638 (2019)
31. Yang, J., Wan, C.L., Zhao, M., Shahid, M., Pan, W.: Effective blocking of radiative thermal conductivity in $La_2Zr_2O_7/LaPO_4$ composites for high temperature thermal insulation applications. J. Eur. Ceram. Soc. **36**, 3809–3814 (2016)
32 Sujith, S.S., Arun Kumar, S.L., Mahesh, K.V., Peer Mohamed, A., Ananthakumar, S.: Sintering and thermal shock resistance properties of $LaPO_4$ based composite refractories. T. Indian Ceram. Soc. **73**, 161–164 (2014)
33. Wang, J.X., Luo, P., Wang, J., Zhan, L., Wei, Y.F., Zhu, Y.M., Yang, S.Y., Zhang, K.B.: Microwave-sintering preparation and densification behavior of sodium zirconium phosphate ceramics with ZnO additive. Ceram. Int. **46**, 3023–3027 (2019)
34. Zhan, L., Wang, J.X., Wang, J., Zhang, X., Wei, Y.F., Yang, S.Y.: Phase evolution and microstructure of new $Sr_{0.5}Zr_2(PO_4)_3$-$NdPO_4$ composite ceramics prepared by one-step microwave sintering. Ceram. Int. **46**, 19822–19826 (2020)
35. ASTM (American Society for Testing and Materials), Standard: C1285–14, standard test methods for determining chemical durability of nuclear, hazardous, and mixed waste glasses and multiphase glass ceramics: the product consistency test (PCT), ASTM International West, Conshohocken, PA, (2014)
36. Pratheep Kumar, S., Gopal, B.: Simulated monazite crystalline waste form $La_{0.4}Nd_{0.1}Y_{0.1}Gd_{0.1}Sm_{0.1}Ce_{0.1}Ca_{0.1}(P_{0.9}Mo_{0.1}O_4)$: synthesis, phase stability and chemical durability study. J. Nucl. Mater. **458**, 224–232 (2015)
37. Buvaneswari, G., Varadaraju, U.: Low leachability phosphate lattices for fixation of select metal ions. Mater. Res. Bull. **35**, 1313–1323 (2000)
38. Rygel, J.L., Pantano, C.G.: Synthesis and properties of cerium aluminosilicophosphate glasses. J. Non Cryst. Solids **355**, 2622–2629 (2009)